



Research article

An integrated radiology-pathology machine learning classifier for outcome prediction following radical prostatectomy: Preliminary findings

Amogh Hiremath^a, Germán Corredor^b, Lin Li^c, Patrick Leo^c,
Cristina Magi-Galluzzi^d, Robin Elliott^e, Andrei Purysko^f, Rakesh Shiradkar^{b,*,**},
Anant Madabhushi^{b,g,*}

^a Picture Health, Cleveland, OH, USA

^b Department of Biomedical Engineering, Emory University and Georgia Institute of Technology, Atlanta, GA, USA

^c Department of Biomedical Engineering, Case Western Reserve University, Cleveland, OH, USA

^d Pathology and Laboratory Medicine Institute, Cleveland Clinic, Cleveland, OH, USA

^e Department of Pathology, University Hospitals Cleveland Medical Center, Cleveland, OH, USA

^f Department of Radiology and Nuclear Medicine, Cleveland Clinic, Cleveland, OH, USA

^g Atlanta Veterans Administration Medical Center, Atlanta, GA, USA

ARTICLE INFO

Keywords:

Prostate cancer
MRI
Histopathology
Machine learning
Prognosis

ABSTRACT

Objectives: To evaluate the added benefit of integrating features from pre-treatment MRI (radiomics) and digitized post-surgical pathology slides (pathomics) in prostate cancer (PCa) patients for prognosticating outcomes post radical-prostatectomy (RP) including a) rising prostate specific antigen (PSA), and b) extraprostatic-extension (EPE).

Methods: Multi-institutional data (N = 58) of PCa patients who underwent pre-treatment 3-T MRI prior to RP were included in this retrospective study. Radiomic and pathomic features were extracted from PCa regions on MRI and RP specimens delineated by expert clinicians. On training set (D1, N = 44), Cox Proportional-Hazards models M_R , M_P and M_{RAP} were trained using radiomics, pathomics, and their combination, respectively, to prognosticate rising PSA (PSA > 0.03 ng/mL). Top features from M_{RAP} were used to train a model to predict EPE on D1 and test on external dataset (D2, N = 14). C-index, Kaplan-Meier curves were used for survival analysis, and area under ROC (AUC) was used for EPE. M_{RAP} was compared with the existing post-treatment risk-calculator, CAPRA (M_C).

Results: Patients had median follow-up of 34 months. M_{RAP} (c-index = 0.685 ± 0.05) significantly outperformed M_R (c-index = 0.646 ± 0.05), M_P (c-index = 0.631 ± 0.06) and M_C (c-index = 0.601 ± 0.071) ($p < 0.0001$). Cross-validated Kaplan-Meier curves showed significant separation among risk groups for rising PSA for M_{RAP} ($p < 0.005$, Hazard Ratio (HR) = 11.36) as compared to M_R ($p = 0.64$, HR = 1.33), M_P ($p = 0.19$, HR = 2.82) and M_C ($p = 0.10$, HR = 3.05). Integrated radio-pathomic model M_{RAP} (AUC = 0.80) outperformed M_R (AUC = 0.57) and M_P (AUC = 0.76) in predicting EPE on external-data (D2).

* Corresponding author. Department of Biomedical Engineering, Emory University and Georgia Institute of Technology, Atlanta, GA, USA.

** Corresponding author.

E-mail addresses: rakesh.shiradkar@emory.edu (R. Shiradkar), anantm@emory.edu (A. Madabhushi).

<https://doi.org/10.1016/j.heliyon.2024.e29602>

Received 7 November 2023; Received in revised form 8 April 2024; Accepted 10 April 2024

Available online 15 April 2024

2405-8440/© 2024 The Authors. Published by Elsevier Ltd. This is an open access article under the CC BY-NC license (<http://creativecommons.org/licenses/by-nc/4.0/>).

Conclusions: Results from this preliminary study suggest that a combination of radiomic and pathomic features can better predict post-surgical outcomes (rising PSA and EPE) compared to either of them individually as well as extant prognostic nomogram (CAPRA).

Abbreviations

PCa	Prostate Cancer
BCR	Biochemical Recurrence
PSA	Prostate-specific Antigen
RP	Radical Prostatectomy
EPE	Extraprostatic extension
H&E	Hematoxylin and Eosin
ML	Machine Learning
3T	3-T
mpMRI	Multi-parametric MRI
ADC	Apparent Diffusion Coefficient
DWI	Diffusion Weighted Imaging
PI-RADS	Prostate Imaging-Reporting and Data System
bpMRI	Bi-parametric MRI
IRB	Institutional Review Board
HIPAA	Health Insurance Portability and Accountability Act
GGG	Gleason Grade Group
CoLLAGe	Co-occurrence of Local Anisotropic Gradient Orientations
rFS	Rising PSA Free Survival
AUC	Area Under the Receiver Operating Characteristic Curve
LASSO	Least Absolute Shrinkage and Selection Operator
CI	Confidence Interval
AI	Artificial intelligence

Key points

1. Radiomics and pathomics carry complementary information for prostate cancer prognosis and integrated radio-pathomic models may better predict prostate cancer outcomes (rising PSA and EPE).
2. The combined radiomics and pathomics classifier was found to generalize on an external dataset in predicting extraprostatic extension.
3. The combination of radiomics and pathomics outperformed pre-existing risk estimators (CAPRA) on an external dataset in our study.

1. Introduction

Prostate cancer (PCa) patients who experience biochemical recurrence (BCR: two consecutive prostate-specific antigen (PSA) measurements >0.2 ng/mL post radical prostatectomy (RP)) have a higher risk of developing metastasis, which in turn is highly associated with PCa-specific mortality [1]. Approximately 20–40 % [2,3] and 30–50 % [4] of patients experience BCR within 10 years post-RP and post-radiotherapy. Additionally, about 24–34 % and 5–10 % of patients with BCR further develop metastasis and die from PCa, respectively [1,5]. Therefore, accurate prediction of BCR post-RP can allow for early identification of high-risk PCa patients who might benefit from adjuvant therapy.

Recently, companion diagnostics have been used to direct adjuvant therapy to only high-risk patients [6]. However, there is an unmet clinical need and a shortage of accurate prognostic tools that can be used post-RP. Several pre- and post-operative nomograms have been developed to predict BCR [7–10]. While these nomograms are driven primarily by PSA, stage, and Gleason grading, previous studies have shown that some of these human pathologist-derived parameters such as Gleason grading are vulnerable to inter-reviewer variability [11].

With recent technological advances in whole-slide imaging [12], the past decade has seen substantial development and growth in

the field of digital pathology. Pathomics is a field of study that aims at computerized image analysis by extraction of high-throughput quantitative features from routinely acquired hematoxylin and eosin (H&E) slides describing glandular and nuclear shape, arrangement, disorder, and tissue texture. Many previous studies have developed machine learning (ML) based approaches using pathomics and have highlighted their prominence in tasks such as predicting the aggressiveness of the tumor via Gleason grade [13,14] and prognosticating BCR [15,16].

With regards to imaging, advancements in 3-T (3T) prostate multi-parametric MRI have improved the detection and characterization of PCa [17,18]. Although Prostate Imaging-Reporting and Data System (PI-RADS) [19] guidelines have been standardized for PCa diagnosis and characterization, previous studies have shown that PI-RADS interpretation is still limited by intra- and inter-reader variability [20]. Radiomics is a quantitative approach in medical imaging that aims to extract and evaluate quantitative features defining attributes such as shape, volume, surface, and texture of a region of interest. Recently, several radiomics-based approaches on bi-parametric MRI (bpMRI: T2-weighted (T2W) and diffusion weighted (DWI)) have been developed, and these studies have demonstrated their ability in PCa diagnosis [21], risk stratification [22,23], and BCR prediction [24,25].

While radiomics can provide insight into anatomical and functional characteristics of a PCa lesion by means of quantifying tumor heterogeneity, their macroscopic resolution limits analysis of in-depth microstructural information. Such microscopic tissue specific attributes including gland and nuclear shape, arrangement, disorder, and tissue texture can be quantified using pathomics. Therefore, radiomic and pathomic features carry complementary information at different scales and we hypothesize that integration of these features can potentially enrich characterization of tumors and enable the construction of a more powerful model for BCR prediction. Consequently, in this work, on multi-site cohort of $N = 58$ ($D1 = 44$, $D2 = 14$) patient studies, we developed and validated an integrated radio-pathomic ML model combining features from pre-treatment bi-parametric MRI and post-surgical prostate H&E slides for prognosticating post-RP outcomes. We note that in our study, of the $N = 44$ patient studies in D1, only 3 experienced BCR while rising PSA (PSA > 0.03 ng/mL) was observed among 13 patients. To ensure a balanced training dataset, we chose to use rising PSA as the outcome of interest as opposed to BCR. Moreover, previous studies have indicated that rising PSA is very strongly associated with BCR

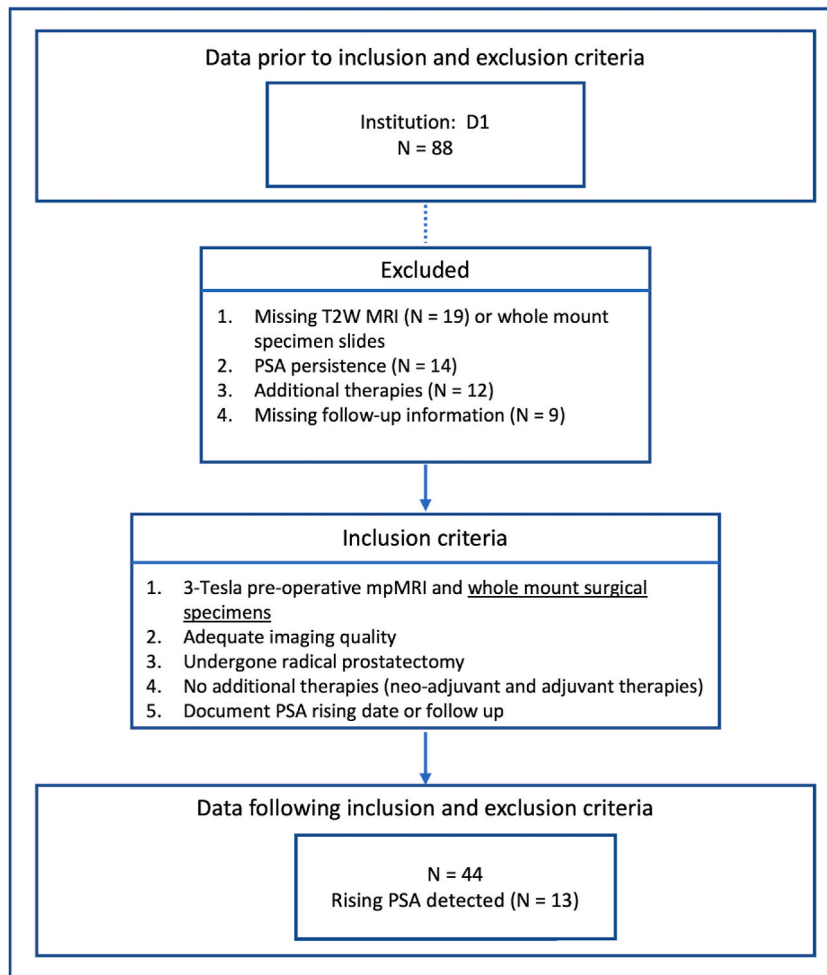


Fig. 1. Flowchart of patient selection for dataset, D1. T2W MRI: T2-Weighted MRI. PSA: Prostate-specific antigen.

(Hazard Ratio (HR) 8.5, $p < 0.0001$) and may be used as a surrogate for BCR.

Additionally, extraprostatic extension (EPE), which refers to presence of tumor cells beyond prostate capsule borders, is considered to be one of the primary adverse pathology findings along with lymph node invasion and seminal vesicle invasion [26]. EPE is also a critical part of the pathological tumor grading process [27], considered a risk factor for poor prognosis and is often included within risk predictors post-RP (HR range, 4.1–5.2) [28]. Furthermore, in some cases, adjuvant radiation therapy is recommended for patients with detected EPE [29]. Although EPE is most commonly detected in RP specimens, pre-operative prostate MRI can sometimes aid in accurate EPE detection [30]. Hence, in this work, we sought to evaluate whether the integrated radiomic and pathomic features that are prognostic of rising PSA are also prognostic of the presence of EPE.

2. Methods

2.1. Study design and participants

This retrospective study included data from two institutions, D1 (N = 44) and D2 (N = 14). A detailed overview of the datasets, including information regarding tumor annotations, is provided below.

2.1.1. Dataset D1

A total of 88 patients from D1 underwent RP between April 18, 2012 to October 2, 2017. The study was approved by the Institutional Review Board (IRB) and was compliant with the Health Insurance Portability and Accountability Act (HIPAA). The need for informed consent for all the patients was waived by the IRB. Access to digitized post-operative whole mount H&E slides and preoperative 3T mpMRI was available for each of these patient studies. Fig. 1 shows the inclusion and exclusion criteria.

A total of 44 patients met the patient selection criteria. Table 1 shows the patient demographic data. Due to limited size, the entire D1 dataset was used for cross-validation. Since only three of 44 patients met the definition of BCR post-RP, this study was focused on identifying patients with rising PSA (rPSA⁺) which was defined as the rise in PSA levels (PSA > 0.03 ng/mL) after being undetectable post-RP.

2.1.1.1. MRI Imaging and prostate cancer delineations on MRI. All patients (N = 44) underwent 3T mpMRI with a surface pelvic phased-array coil. Table S1 presents the detailed MRI acquisition parameters. A radiologist with more than 10 years of experience reviewed the mpMRI scans and manually delineated the PCa lesions on T2W MRI with RP specimens as reference. The delineations on MRI were made on all axial slices (each 2D axial slice with the presence of a lesion was annotated) of T2W MRI using an open-source software, 3D Slicer [31]. Only the index lesions, defined as the lesion with the highest Gleason grade group (GGG) from each patient, were included for radiomic analysis.

Additionally, to evaluate the stability and repeatability of the radiomic features, we used a Quantitative Imaging Network-PROSTATE-Repeatability dataset [32] (QIN test-retest dataset) from The Cancer Imaging Archive, consisting of baseline and repeat prostate multiparametric MRI scans of 15 individuals taken 2 weeks apart. Among the 15 patients, a suspected tumor was identified in 11 patients. One patient was excluded due to the poor quality. The repeatability of radiomic features was assessed based on the remaining 10 patients.

2.1.1.2. Whole mount H&E slides and prostate cancer delineations on H&E slides. All whole mount specimens were weighed, fixed in formalin, and serially sectioned at 3 mm intervals. Samples were divided into quadrants and digitized on an Aperio AT Turbo scanner at 20× magnifications (0.4960 microns-per-pixel). The slide containing the index lesion (highest grade/tumor) was annotated for a representative tumor region by an experienced genitourinary pathologist (>10 years of experience) and features were extracted from this region using the Aperio ImageScope software.

Table 1

Patient demographic information. IQR: Interquartile range. PSA: Prostate-specific antigen. GGG: ISUP Gleason grade group. PZ: peripheral zone. TZ: Transitional zone. rPSA⁺: Rising PSA. rPSA⁻: No rising PSA.

Parameter	Description (Value)				
#Patients	N = 44				
Age (years) (median (IQR))	62 (57–65.25)				
PSA (ng/ml) (median (IQR))	5 (4.31–6.99)				
Prostate Volume (mm ³) (median (IQR))	33.05 (29.05–45.73)				
PSA Density (ng/ml/mm ³) (median (IQR))	0.14 (0.1–0.21)				
Pathologic GGG (# patients)	1	2	3	4	5
	1	26	9	2	6
PI-RADS v2 (# lesions)	1	2	3	4	5
	1	8	3	8	24
Zone (# lesions)	PZ		TZ		
	32		12		
Rising PSA # patients	rPSA-		rPSA+		
	31		13		

2.1.2. Dataset D2

The D2 dataset is a publicly available dataset from the TCIA, Fused Radiology-Pathology Prostate Dataset (Prostate Fused-MRI-Pathology) [33]. The D2 dataset comprises 28 patients with pre-treatment prostate multi-parametric MRI and digitized H&E images of corresponding RP specimens. Detailed descriptions of the dataset can be found in previously published studies [34–37]. Since only 14 of 28 patients had tumor annotations on both T2W-MRI and H&E, only these patients were included in this study.

2.2. Feature extraction

Radiomic and pathomic features were extracted from bpMRI and whole-mount H&E slides, respectively.

2.2.1. Radiomic feature extraction

Radiomic features were extracted from both T2W MRI and apparent diffusion coefficient (ADC) maps derived from diffusion weighted imaging (DWI). As part of the T2W MRI preprocessing step, a non-parametric intensity standardization method [38] was used to correct for intensity drift artifacts and normalize the T2W MRI to a particular range. The T2W MRI was further resampled to a uniform axial resolution of 0.5 mm × 0.5 mm.

Since annotations were only performed on T2W MRI, we co-registered the ADC images to T2W MRI. A rigid followed by affine registration with a multiresolution framework of *elastix* [39] was used for registration. Control points from the entire field of view were used for rigid registration while those from the prostate capsule alone were used for affine registration. Mattes mutual information was used as the similarity metric with the number of histogram bins set to 32 [40]. The similarity metric was optimized using gradient descent, with a maximum of 500 iterations per resolution. A linear interpolator was used.

Subsequently, radiomic features (N = 2200) including first-order statistics, Gray Level Co-occurrence Matrix (GLCM), Gray Level Size Zone (GLSZM), Gray Level Run Length Matrix (GLRLM), and Gray Level Dependence Matrix (GLDM) as part of pyradiomics package [41] with additional features, including Co-occurrence of Local Anisotropic Gradient Orientations (CoLLAGE) [42], Laws [43] and Gabor [44] were extracted from PCa ROIs on T2W MRI and the co-registered ADCs. The radiomic feature extraction in this study was performed using pyradiomics [41] with additional features and image filters (CoLLAGE, Laws, Gabor) implemented.

2.2.2. Pathomic feature extraction

As part of the pathomic feature extraction preprocessing step, all H&E images were first resized to a resolution of 1 micron-per-pixel (×10 magnification) resolution. Glands present within the cross-section of H&E images are generally composed of lumen in the center with epithelial nuclei at the boundary and cytoplasm filling in the intermediate space. Quantification of glandular shape and arrangement first requires accurate segmentation of the lumen. Therefore, in this work, the lumen was segmented using a previously trained U-Net model [15], and features were extracted based on the segmented lumen. Five different families with a total of 242 pathomic features were extracted; Descriptions of each of them are provided below;

Global graph: These features were derived from lumen centroid coordinates and they include descriptors of gland arrangement and density-derived measurements from the edges and polygons of Voronoi and Delaunay maps [14,45]. They constituted 51 features among a total of 242.

Lumen shape: These descriptors included lumen shape-based features with 25 shape measurements including invariant and Fourier descriptors of boundary points, fractal dimension, smoothness, area, and perimeter and their corresponding statistics (mean, median standard deviation, 5th/95th percentile) [14,45] for a total of 100 features.

Lumen orientation disorder: A total of 39 features of lumen orientation disorder features describing how chaotic the glands appear in an image were extracted. A co-occurrence matrix was constructed for every sub-graph in an image and measures of entropy, variance, and energy were extracted from the matrix [16]. 18 × 18 co-occurrence matrix based on lumen orientation angles binned in the intervals of 10° between 0 and 180° was used for the feature extraction.

Sub-graph: A total of 26 descriptors describing local gland arrangement, packing, and clustering were extracted. These features included sub-graph radius, eccentricity, clustering, path length, the ratio of glands in the largest sub-graph to the total number of glands, and the percentage of glands that are isolated [46].

Harlick: These descriptors were based on pixel intensity. The entire region of interest was converted into a grayscale image and 39 Haralick features [47] describing the texture, edges, gradients, spots, and homogeneity of the image were extracted. The pathomic feature extraction was performed using an in-house MATLAB V.2019 (MathWorks, Natick, Massachusetts, USA) toolbox.

2.3. Machine learning models for prognosticating rising PSA

On dataset D1, Cox Proportional-Hazards (CPH) (*CoxnetSurvivalAnalysis model implementation from scikit-survival python package* [48]) ML classifiers M_R (T2W MRI and ADC features) and M_P (H&E features) were trained separately with extracted radiomic and pathomic features respectively for prognosticating rising PSA. An additional CPH model, M_C , was trained with scores from a pre-existing post-operative risk estimator, CAPRA [49]. CAPRA is a risk predictor that assesses risk of PCa outcomes post-RP. It accounts for factors such as PSA levels, Gleason score, clinical stage, and age and was developed and validated using Cox proportional hazards and life table analysis [49]. A 10-fold cross-validation strategy with 300 iterations of stratified random splits was used to optimize M_R and M_P . At each iteration of cross-validation, the following feature processing strategy was adopted; At first intraclass correlation coefficients (ICC) for the entire set of features of T2W MRI and ADCs between the baseline and repeat scans of QIN test retest were calculated. Features with ICC < 0.8 were removed from the analysis owing to their low repeatability score. Subsequently,

correlated features with a Pearson correlation >0.9 and constant features which were repeated for more than 25 % of the samples were removed. Next, an outlier removal was performed clipping the feature values between 1 and 99 percentiles. Subsequently, features were normalized to a range $[0,1]$ using min-max normalization, and a feature selection method was used to select the top features.

Fig. 2 depicts the ML framework of a fused classifier (M_{RaP}) combining M_R and M_P . A similar 300 iteration and 10-fold cross-validation strategy as defined for the individual classifiers M_R and M_P were used to train a fused radiomic and pathomic CPH model, M_{RaP} . The final fused CPH classifier, M_{RaP} , was constructed by taking average prediction probabilities from M_R and M_P .

Subsequently, the top radiomic and pathomic features (based on the frequency of the features selected within the cross-validation) from M_R and M_P respectively were further used to train logistic regression classifiers E_R (only top T2W MRI radiomic features), E_P (only top pathomic features) and E_{RaP} (top radiomic and pathomic features) on D1, and test on external data (D2) to predict EPE.

The training of machine learning classifiers, including feature normalization, preprocessing, and cross-validation, was performed using the scikit-learn (version 0.24.1) and scikit-survival (0.19.0) modules in Python (version 3.9).

2.4. Statistical analysis

The rising PSA-free survival (rFS) period is defined as the interval between RP and the date PSA began rising for the patient. For patients without rising PSA (rPSA⁻), the last reported follow-up was labeled as censored. We used mean \pm standard deviation of the c-index and area under the receiver operating characteristic curve (AUC) for evaluating the cross-validation accuracy of CPH models (M_R , M_P , M_{RaP}). Two different feature selection strategies, including penalized cox-regression models with Least Absolute Shrinkage and Selection Operator [50] (LASSO) penalty on survival data (time from surgery to rising PSA or last follow-up date), and LASSO on binary censor data (whether had rising PSA or not), were tested. Following the 1 in 10 rule adopted in many previous studies [51,52], we limited the number of features (n_f) to approximately 10 % of samples to avoid the risk of overfitting. Hence, cross-validation was repeated by considering the number of features = $1, 2 \dots n_f$. The best configuration (b_c) with a particular feature selection strategy (b_{fs}) and number of features (b_{nf}) was decided based on the highest mean \pm standard c-index over 300 iterations of 10-fold cross-validation. Further details of the evaluation strategy for cross-validation are provided in the supplementary section, S1. Subsequently, on the best combination (b_c), cross-validated Kaplan-Meier survival curves [53,54] were generated for time-to-event analysis. Hazard ratios with

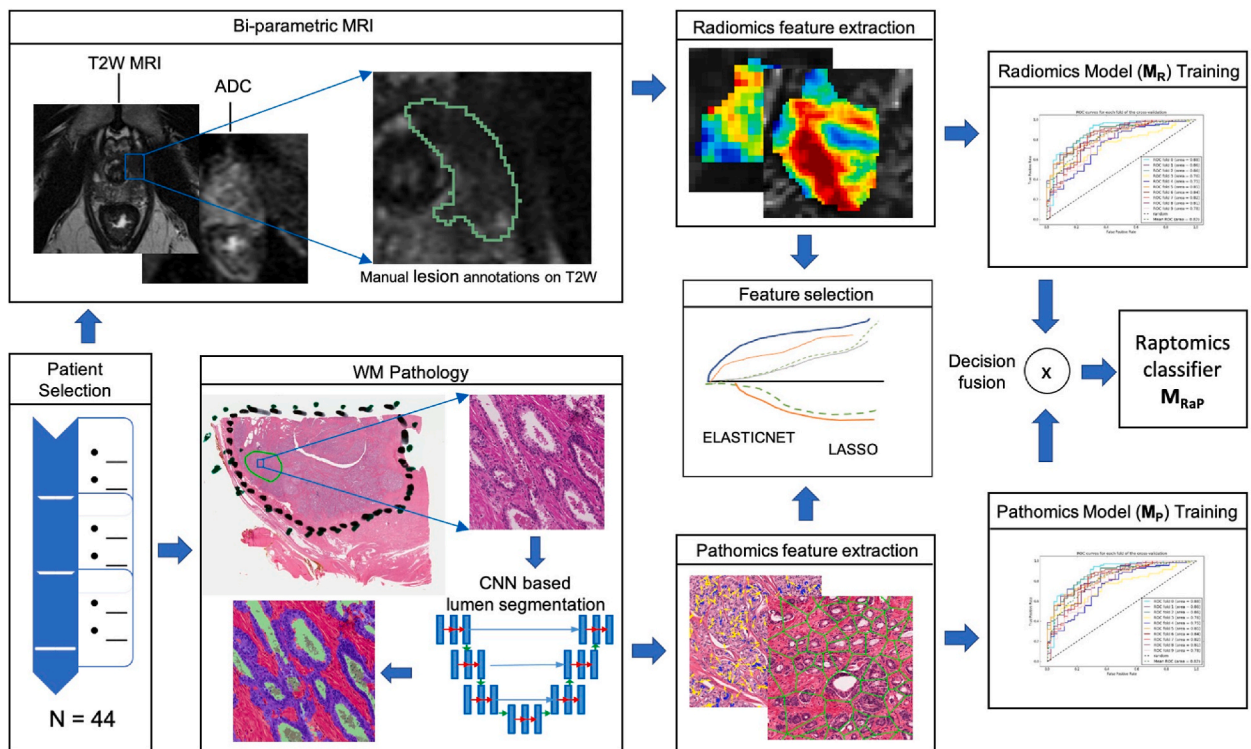


Fig. 2. Machine learning pipeline for the fused radiomics-pathomics Cox-Proportional Hazard (CPH) classifier constructed by integrating a radiomic-based CPH classifier (M_R) and a pathomics-based CPH classifier (M_P). For M_R , at first T2W MRI is manually annotated, and radiomic features are extracted from within the annotated lesion on T2W MRI and co-registered ADCs. Subsequently, top features are selected and the CPH model is trained to prognosticate rising PSA. Similarly, for M_P the digitized H&E slides are first manually annotated, and lumen segmentation is performed within the annotated region. Subsequently, pathomic features are extracted within the region of interest, followed by feature selection and training of a CPH model to prognosticate rising PSA. Finally, the predictions of M_R and M_P are fused (average of prediction probabilities) at the decision fusion node to create a fused radiomics-pathomics classifier, M_{RaP} .

95 % confidence intervals were reported for each classifier. Additionally, log-rank tests were used to determine statistically significant differences ($p < 0.05$) in rising PSA-free survival (rFS). Furthermore, AUC was used as a metric to evaluate classifiers predicting EPE on the external dataset (D2).

3. Results

3.1. Study participants

In D1, patients had a median follow-up data of 34 months. Among these 44 patients, rising PSA was detected in 13 patients, of which three went on to experience BCR as per the standard definition. Additionally, 19 of 44 patients in D1 and seven of 14 patients in D2 presented EPE post-RP. Within D1, of 13 patients with detected rising PSA, 10 had EPE. [Table 1](#) provides further information on patient demographics for D1.

3.2. Experimental results

3.2.1. Performance of individual radiomics, pathomics, and CAPRA models

Since the training dataset D1 included 44 patients, configurations of classifiers M_R and M_P were set with a maximum number of features to be approximately 10 % of the samples ($n_f = 5$) to avoid overfitting [51,52]. Supplementary Table S2 shows the mean \pm standard deviation of the c-index of different configurations of M_R and M_P over 300 iterations of 10-fold cross-validation. M_R resulted in a cross-validation C-index of 0.646 ± 0.05 and the best configuration (\mathbf{b}_c) for M_R was found to be; $\mathbf{b}_{fs} =$ LASSO penalized cox-regression on censor data; and $\mathbf{b}_{nf} = 1$. Similarly, M_P resulted in a cross-validation C-index of 0.631 ± 0.06 with the best configuration (\mathbf{b}_c) for M_P was found to be; $\mathbf{b}_{fs} =$ LASSO on survival data and $\mathbf{b}_{nf} = 4$. Supplementary Figs. S1 and S2 depict the frequencies of features selected for the best configuration of M_R and M_P respectively. The top features that were selected for M_R were based on CoLIAGE [42] gray level cooccurrence (GLCM) family of features from the ADC. Similarly, among the four top features that were selected for M_P , one feature was based on a sub-graph, and three features were based on lumen shape. [Table 2](#) shows a univariate cox regression analysis of the selected radiomic and pathomic features. A CoLIAGE radiomic feature and a gland-shaped pathomic feature were found to be most strongly associated with rising PSA using univariate analysis. No significant separation was observed for cross-validated Kaplan-Meier survival curves ([Fig. 3](#)) for M_R ($p = 0.64$, HR = 1.33) and M_P ($p = 0.19$, HR = 2.82). A CPH model, M_C trained on CAPRA scores [49] yielded a cross-validation c-index of 0.601 ± 0.071 with cross-validated Kaplan-Meier survival curves ([Fig. 3](#)) not showing significant separation between rPSA⁻ and rPSA⁺ patients ($p = 0.10$, HR = 3.05).

3.3. Performance of combined radiomics and pathomics-based models

M_{RAP} yielded a mean \pm standard deviation c-index of 0.685 ± 0.05 and was found to outperform both M_R , M_P , and M_C ($p < 0.0001$). From the cross-validated Kaplan-Meier survival curves ([Fig. 3](#)) it can be observed that M_{RAP} showed significant separation between patients with and without rising PSA ($p < 0.005$, HR = 11.36). Additionally, [Fig. 4](#) illustrates the corresponding visualizations of one of the top features of M_R (original_collage2D_glcMv_JointEnergyEntropy) and M_P (Shape: 5 %/95 % invariant 1). The presence of more chaotic intensity gradient orientations quantified by CoLIAGE radiomic feature on ADC ([Fig. 4](#): R3, R4) suggests more aggressive PCa with a higher risk of rising PSA as compared to the ones with more uniform and lower entropy regions ([Fig. 4](#): R1, R2). Similarly, the pathomic visualizations of Shape: 5 %/95 % invariant 1 (a gland shape feature) illustrates that high-risk rising PSA patients with aggressive cancer may present uniformly small, malformed lumen, resulting in lower 5th/95th percentile ratios (lower range) ([Fig. 4](#): P3, P4) as compared to cases with lower risk of rising PSA ([Fig. 4](#): P1, P2).

Additionally, when top radiomic features from M_R (including only T2W MRI features: a GLCM and two Gabor-based based features) and M_P were used to train classifiers E_{RAP} (trained using combination of top radiomic and pathomic features on D1), E_R (trained with top radiomics features extracted solely from D1) and E_P (trained with top pathomic features solely from D1), E_{RAP} (AUC = 0.80) was found to outperform E_R (AUC = 0.57) and E_P (AUC = 0.76) on the external dataset, D2. [Fig. 5](#) shows the comparison of E_R , E_P , and E_{RAP} through a receiver operating characteristic (ROC) curve.

Table 2

Univariate cox regression analysis of selected radiomic and pathomic variables through LASSO and elasticnet feature selection methods. The first feature represents the top radiomic feature and belongs to the Co-occurrence of Local Anisotropic Gradient Orientations (CoLIAGE) gray level cooccurrence matrix (GLCM) family of features. Rows 4–7 represent the top pathomic features. One sub graph feature and three gland shape-based features were the top pathomic features. * indicates statistical significance ($p < 0.05$) in univariate analysis.

	Feature	Log hazard ratio	p-value
1	collage2D_glcMv_JointEnergyEntropy_ADC	0.16	0.01*
2	CGT: Std. tensor contrast energy	2.91	0.13
3	Shape: 5 %/95 % invariant 7	0.01	1.00
4	Shape: 5 %/95 % invariant 1	4.80	0.04*
5	Shape: Mean Fourier 10	2.81	0.14

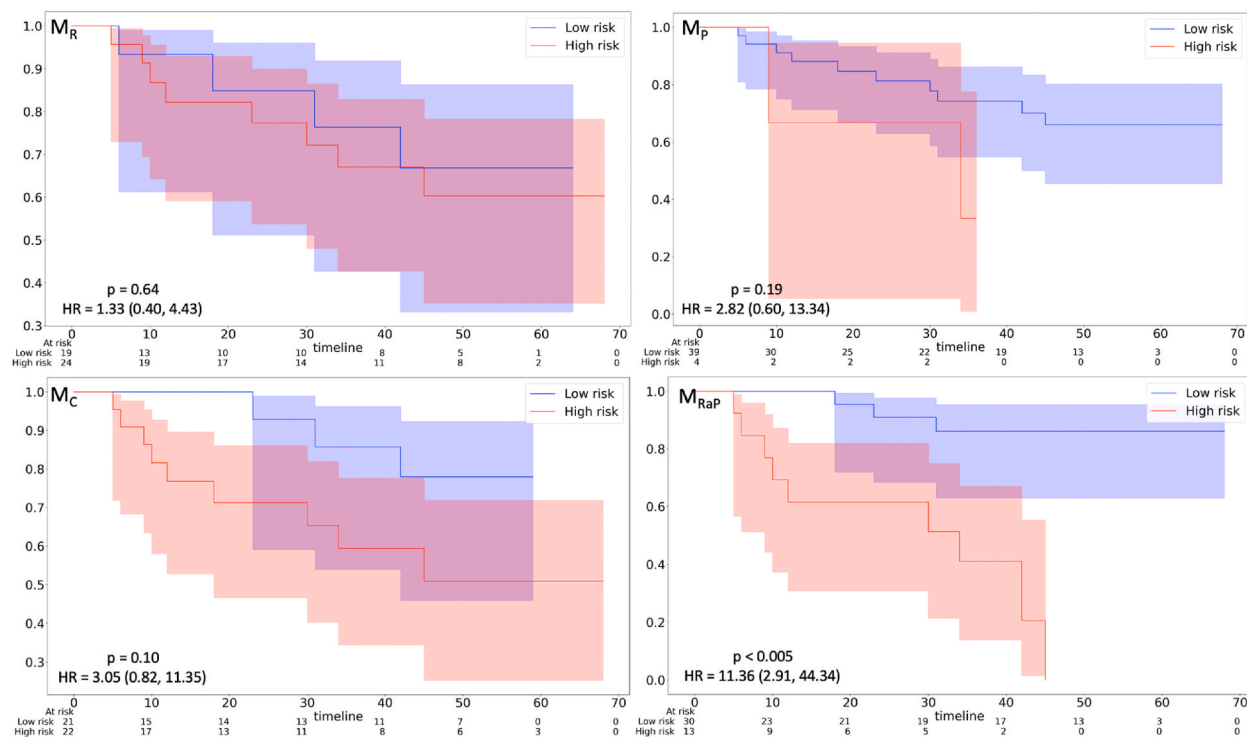


Fig. 3. Cross-validated Kaplan-Meier curves for radiomics Cox-Proportional Hazard (CPH) model (A: M_R), pathomics CPH model (B: M_P), CAPRA (C: M_C) and the fused radiomics-pathomics model (D: M_{RaP}). One can notice that these cross-validated Kaplan-Meier curves show significant separation for M_{RaP} ($p < 0.005$, Hazard Ratio (HR) = 11.36) as compared to M_R ($p = 0.64$, HR = 1.33), M_P ($p = 0.19$, HR = 2.82) and M_C ($p = 0.10$, HR = 3.05).

4. Discussion

Among the various clinical endpoints after radical prostatectomy (RP) in prostate cancer (PCa) patients, biochemical recurrence (BCR) is usually the first evidence of tumor recurrence [5]. BCR presents a major progression and is known to be associated with a significant risk of metastasis and PCa-specific mortality [1,2]. Adjuvant therapies, given in the form of radiation therapy or chemotherapy with drugs such as docetaxel, have previously been shown to be effective in reducing risk of metastasis or PCa-specific death [55,56]. However, adjuvant therapy is not appropriate for all patients due to the low overall mortality of PCa patients [57]. Therefore, accurate prediction of PCa patients with a higher risk of BCR can help identify ideal candidates for adjuvant therapy. Additionally, extraprostatic extension (EPE) identified from RP specimens and prostate MRI has previously been shown to be associated with a higher risk of BCR [58]. Hence, accurate detection of EPE among RP patients can help triage patients for further adjuvant treatments such as radiation therapy.

In the last decade, there has been an increased interest in the use of genomic signatures in predicting different outcomes [59,60]. One such genomic risk classifier, Decipher, has been widely used and validated for predicting the risk of metastasis and PCa-specific mortality [61,62]. However, these tests are tissue-destructive, which limits the test from being performed multiple times. Specifically, in cases with small tumors, tissue can be exhausted with repeated testing.

In this work, we developed a fused radiomics and pathomics Cox-Proportional Hazard model (M_{RaP}) by combining signatures from pre-treatment prostate bpMRI and post-RP digitized H&E slides to prognosticate rising-PSA post-RP and showed that M_{RaP} outperformed its individual counterparts (M_R and M_P). Additionally, by using the top radiomic and pathomic features from the rising PSA model, we further trained a classifier to predict EPE. On the external validation dataset, D2, the fused radiomics and pathomics model (E_{RaP}) was found to outperform the individual classifiers E_R and E_P in predicting EPE among RP patients.

Artificial intelligence (AI) based approaches on prostate MRI are widely being explored for PCa risk stratification [23,63,64] and BCR prediction [24,25]. For instance, specifically in the context of BCR prediction, Shiradkar et al. [24] and Bourbonne et al. [25] showed that machine learning (ML) classifiers trained with radiomic features were predictive of BCR. Corroborating the findings of Shiradkar et al. [24], the radiomic classifier M_R in our study also resulted in identifying CoLIAGE entropy feature from ADC as a top feature associated with the risk of BCR. CoLIAGE features measure the local intensity gradient patterns within images, providing a quantification method to capture gradient based heterogeneity of tumors. Previous studies have demonstrated an association between tumor heterogeneity and hypoxic microenvironment. The variations in hypoxia-related heterogeneity might be reflected in the distinct expression patterns of CoLIAGE entropy [42]. While radiomic-based models from previous studies yielded HR = 1.9, 95 % CI [1.4–2.7],

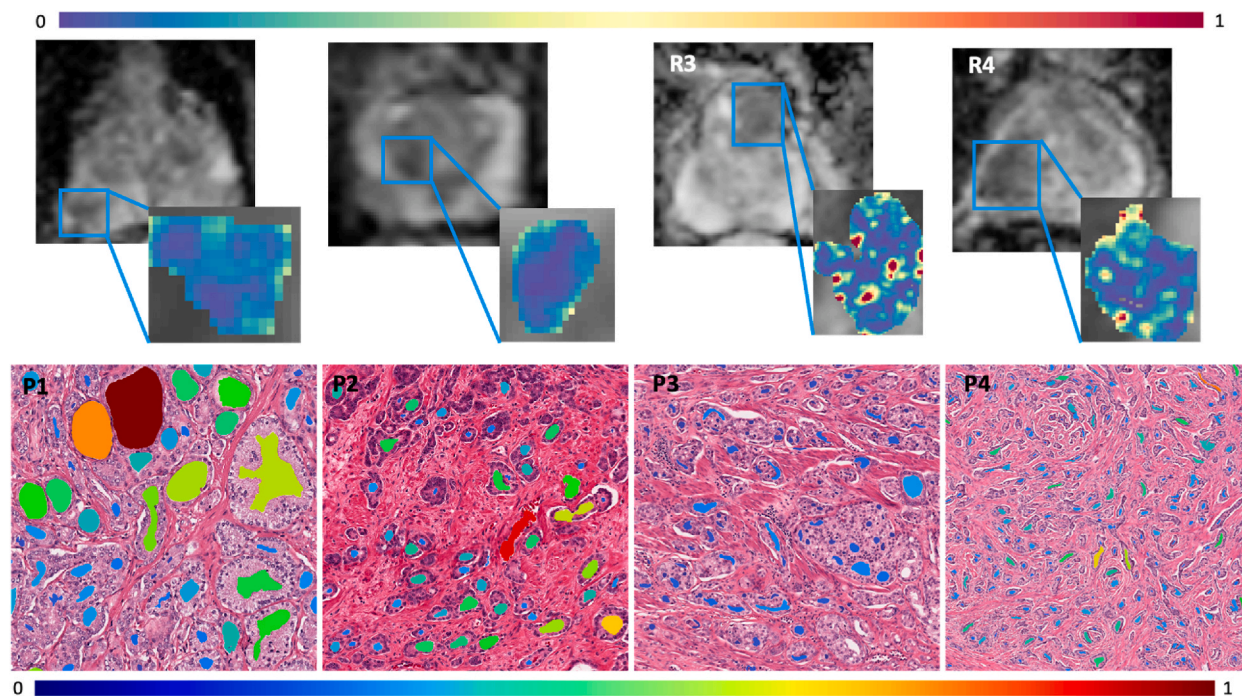


Fig. 4. Visualizations of one of the topmost features of M_R (original_collage2D_glcM_V_JointEnergyEntropy) (R1-R4) and M_P (Shape: 5 %/95 % invariant 1) (P1–P4) between four different patients. The columns 1,2 represent patients with a low risk of rising PSA and columns 3,4 represent patients with a high risk of rising PSA. It can be observed that the visualizations of Co-occurrence of Local Anisotropic Gradient Orientations (CoLIAGE) gray level cooccurrence matrix (GLCM) radiomic feature on apparent diffusion coefficient (ADC) maps indicates the presence of higher density of high entropy regions for which M_R has classified as $rPSA^+$ (Fig. 4: R3, R4), as compared to the ones for which M_R has classified as $rPSA^-$ (Fig. 4: R1, R2). Similarly, the pathomic visualizations of Shape: 5 %/95 % invariant 1 depicts that a high risk of rising PSA with more aggressive cancer leads to uniformly small, malformed lumen resulting in a lower 5th/95th percentile ratio (lower range) (Fig. 4: P3, P4) as compared to cases with lower risk of rising PSA (Fig. 4: P1, P2). For radiomic visualizations, the feature array output from the pyradiomics package was used to overlay on top of the ADC using matplotlib package. For pathomic visualizations, in-house MATLAB code was used to overlay the visualizations.

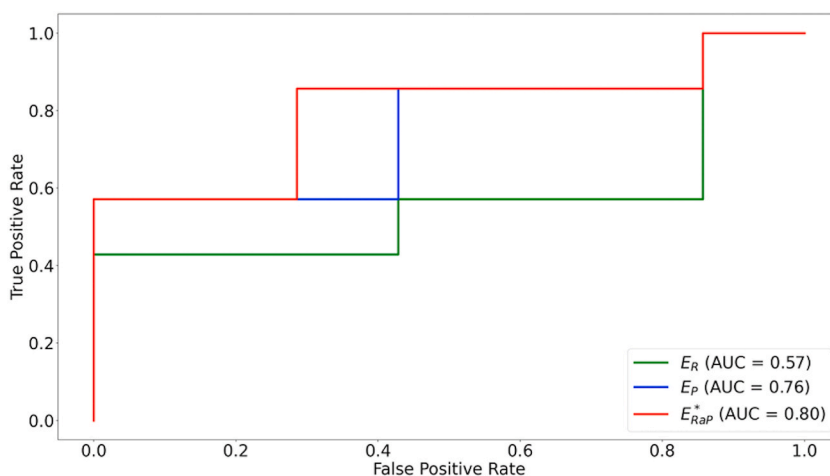


Fig. 5. Area under the receiver operating characteristic curve (AUC) comparison of machine classifiers $E_{R_{ap}}$ (trained using combination of top radiomic and pathomic features on D1), E_R (trained with top radiomics features extracted solely from D1) and E_P (trained with top pathomic features solely from D1).

$p < 0.05$ [65] and $HR = 2.91$, 95 % CI [1.45–11.51], $p = 0.02$ [66] for predicting risk of BCR respectively, in this study we demonstrated that combining radiomic and pathomic features can separate low risk and high risk rising PSA patients with $HR = 11.36$, 95 % CI [2.91–44.34].

Similarly, in the context of whole slide imaging, several previous AI-based studies have demonstrated the prominence of pathomic features for various tasks, such as automated Gleason grading [13,14] and predicting the risk of BCR [15,67]. In this study, we trained an ML classifier (M_p) using pathomic features derived from whole slide images. Among five different families of pathomic features, three gland shape-based features, and one sub-graph-based feature were found to be the topmost ones. These features were also previously found to be selected as top features in previous [15,16]. Pathomic feature visualizations of one of the top pathomic features, Shape: 5 %/95 % invariant 1 (Fig. 4) depicts that high risk of rising PSA with more aggressive cancer leads to uniformly small, malformed lumen resulting in lower 5th/95th percentile ratio (lower range) (Fig. 4: P3, P4) as compared to cases with lower risk of rising PSA (Fig. 4: P1, P2). Additionally, while machine learning models from previous studies using pathomic features for BCR prediction among PCa patients yielded HR = 2.83, 95 % CI [2.03–3.93] [15], our combined radiomics and pathomics model was able to separate low-risk and high-risk rising PSA patients with HR = 11.36, 95 % CI [2.91–44.34].

While some groups have begun to develop and apply approaches for combining image features from radiology and pathology scans [68–70], these approaches have not yet been applied to PCa characterization. Feng et al. [68], Rathore et al. [70] and Vaidya et al. [69] illustrated that combining signatures from both radiology and histopathology can help in the better prognosis of rectal cancer, glioblastoma, and early-stage lung cancers. Additionally, studies have also developed signatures integrating genomics (quantifying cellular activities measured at the molecular level) either with pathomics [71] or with both radiomics and pathomics [72] for predicting various disease outcomes.

However, in the context of PCa, a few studies have made attempts to integrate pathology with radiology [73,74] through spatial co-registration and correlating radiomic and pathomic features. For instance, McGarry et al. [73] co-registered whole mount specimens to T2W MRI and trained a regression algorithm to predict epithelium density values using T2W MRI intensities using pathologist-delineated regions of interest. Additionally, in a previous study, correlations between whole-mount specimens and T2W MRI were assessed by co-registering whole-mount specimens to MRI and mapping pathologist-identified regions of interest on MRI [74]. However, our work involved identifying the top features in each modality, i.e., radiology and pathology, separately and integrating them to create a fused super-classifier for improved prognostication compared to radiology and pathology alone.

The uniqueness of our approach was to focus on demonstrating the added benefit of combining interpretable and biologically explainable hand-crafted radiomic and pathomic features which have previously shown promise in prognosticating BCR when used separately. While deep learning fusion strategies of radiology and pathology have been previously used for disease characterization [72,75,76], their black-box nature and lack of interpretability among these models hinders their ability to explain the biological underpinning of the disease. Mobadersany et al. [75] and Chen et al. [76] combined histopathology with genomics, and Braman et al. [72] combined radiology in addition to histopathology and genomics via deep learning frameworks to illustrate that the fusion approaches outperform their individual counterparts. In this work, on a discovery cohort (N = 44 patients), we demonstrated the added benefit of combining interpretable radiomic- and pathomic-based ML models for predicting rising PSA. Through feature visualizations we explained the biological phenomena associated with the features. Additionally, for EPE as an endpoint, we also demonstrated that the fused radiomics-pathomics E_{Rap} classifier is a significant improvement over the individual classifiers E_R and E_p , each trained with only radiomic and pathomic features.

Our study did have its limitations. This preliminary study involved only 44 patients with rising PSA endpoints. While cross-validation was a reasonable strategy to generate the preliminary findings for this proof-of-concept study, to prove the clinical utility of the approach it is necessary to validate the presented approach on external test sets from multiple sites, as well as perform prospective validation. However, with EPE as an endpoint, we demonstrated that the fusion of radiomics and pathomics provides significant improvement over the individual data streams, not only on the discovery cohort but also on an external dataset. Furthermore, as previously discussed, since only three of the 44 patients had BCR, we chose rising PSA (PSA > 0.03 ng/mL) as the clinical endpoint. However, previous studies have shown that rising PSA is an independent factor that identifies BCR more accurately than any traditional risk factors and presents a significant lead-time advantage [77]. Additionally, this study focuses on demonstrating the added benefit of combining previously used radiomic and pathomic features while introducing novel hand-crafted features and exploring other interpretable deep learning approaches remain part of future directions. Lastly, the current biomarkers in this study are only prognostic of rising PSA; however, identifying predictive biomarkers remains part of future work.

In conclusion, the results of this proof-of-concept study suggest that an integrated radiomics-pathomics approach combining representations from both radiology (prostate MRI) and pathology (whole mount H&E slides) can help better prognosticate rising PSA and identify EPE, as compared to radiology and pathology alone. Furthermore, this fusion-based approach can potentially be used as an alternative to more expensive and tissue-destructive assays like Decipher.

Ethics statement

This study was reviewed and approved by the Institutional Review Board at Emory University, with the approval number: STUDY00005353.

Informed consent was not required for this study because this study uses de-identified and retrospective data was used with minimal/no risk to patient.

Consent for publication

All co-authors have read the manuscript and approve of its submission to the journal.

Data availability statement

The data associated with the study has not been deposited into a publicly available repository. The authors do not have permission to share data. Requests to access the datasets from Cleveland Clinic (used with permission for this study) should be made directly to the institutions via their data access request forms. We have included the code for model training and evaluation on GitHub (<https://github.com/amogh3892/An-Integrated-Radiology-Pathology-ML-Classifer-post-Radical-Prostatectomy>).

CRedit authorship contribution statement

Amogh Hiremath: Writing – review & editing, Writing – original draft, Software, Methodology, Conceptualization. **Germán Corredor:** Writing – review & editing, Visualization, Formal analysis, Conceptualization. **Lin Li:** Writing – review & editing, Formal analysis, Conceptualization. **Patrick Leo:** Writing – review & editing, Formal analysis, Conceptualization. **Cristina Magi-Galluzzi:** Data curation. **Robin Elliott:** Data curation. **Andrei Purysko:** Data curation. **Rakesh Shiradkar:** Writing – review & editing, Supervision, Methodology, Formal analysis, Conceptualization. **Anant Madabhushi:** Writing – review & editing, Supervision, Software, Resources, Formal analysis, Conceptualization.

Declaration of competing interest

Dr. Anant Madabhushi is an equity holder in Elucid Bioimaging and in Inspirata Inc. In addition, he has served as a scientific advisory board member for Inspirata Inc, Astrazeneca, Bristol Meyers-Squibb and Merck. Currently he serves on the advisory board of Aiforia Inc. He also has sponsored research agreements with Philips, AstraZeneca and Bristol Meyers-Squibb. His technology has been licensed to Elucid Bioimaging. He is also involved in a NIH U24 grant with PathCore Inc, and 3 different R01 grants with Inspirata Inc (NIH 1R01CA202752-01A1: Computerized histologic image predictor of cancer outcome, NIH 1 R01 CA216579-01A1: Computerized Histologic Risk Predictor (CHiRP) for Early Stage Lung Cancers, NIH 1 R01 CA220581-01A1: Quantitative Histomorphometric Risk Classifier (QuHbIC) in HPV + Oropharyngeal Carcinoma). Dr. Andrei Purysko: service contract with Profound Medical and Research support from RSNA R&E foundation. Dr. Patrick Leo is employed in Genentech and have Roche group stock.

Funding and Acknowledgements

This work is made possible by the National Cancer Institute under award numbers R01CA249992-01A1, R01CA202752-01A1, R01CA208236-01A1, R01CA216579-01A1, R01CA220581-01A1, R01CA257612-01A1, U01CA239055-01, U01CA248226-01, U54CA254566-01, National Heart, Lung and Blood Institute R01HL151277-01A1, R01HL158071-01A1, National Institute of Biomedical Imaging and Bioengineering R43EB028736-01, National Center for Research Resources under award number C06 RR12463-01, VA Merit Review Award IBX004121A from the United States Department of Veterans Affairs Biomedical Laboratory Research and Development Service, the Office of the Assistant Secretary of Defense for Health Affairs, through the Breast Cancer Research Program (W81XWH-19-1-0668), the Prostate Cancer Research Program (W81XWH-15-1-0558, W81XWH-20-1-0851), the Lung Cancer Research Program (W81XWH-18-1-0440, W81XWH-20-1-0595), the Peer Reviewed Cancer Research Program (W81XWH-18-1-0404, W81XWH-21-1-0345), the Kidney Precision Medicine Project (KPMP) Glue Grant, DoD Prostate Cancer Research Program Idea Development Award W81XWH-18-1-0524, Clinical and Translational Science Collaborative (CTSC) Cleveland Annual Pilot Award 2020 UL1TR002548 and sponsored research agreements from Bristol Myers-Squibb, Boehringer-Ingelheim, Eli-Lilly and Astrazeneca, DoD Peer Reviewed Cancer Research Program (W81XWH-22-1-0236), Winship Invest\$ Pilot Grant, American Cancer Society Institutional Research Grant from the Winship Cancer Institute. Mike Slive Foundation for Prostate Cancer Research Grant, NCI U01CA113913, NIH AIM-AHEAD Consortium Development Program.

Appendix A. Supplementary data

Supplementary data to this article can be found online at <https://doi.org/10.1016/j.heliyon.2024.e29602>.

References

- [1] S.A. Boorjian, R.H. Thompson, M.K. Tollefson, L.J. Rangel, E.J. Bergstralh, M.L. Blute, R.J. Karnes, Long-term risk of clinical progression after biochemical recurrence following radical prostatectomy: the impact of time from surgery to recurrence, *Eur. Urol.* 59 (2011) 893–899, <https://doi.org/10.1016/j.eururo.2011.02.026>.
- [2] S.J. Freedland, E.B. Humphreys, L.A. Mangold, M. Eisenberger, F.J. Dorey, P.C. Walsh, A.W. Partin, Risk of prostate cancer-specific mortality following biochemical recurrence after radical prostatectomy, *JAMA* 294 (2005) 433–439, <https://doi.org/10.1001/jama.294.4.433>.
- [3] K.A. Roehl, M. Han, C.G. Ramos, J.A.V. Antenor, W.J. Catalona, Cancer progression and survival rates following anatomical radical retropubic prostatectomy in 3,478 consecutive patients: long-term results, *J. Urol.* 172 (2004) 910–914, <https://doi.org/10.1097/01.ju.0000134888.22332.bb>.
- [4] P.A. Kupelian, A. Mahadevan, C.A. Reddy, A.M. Reuther, E.A. Klein, Use of different definitions of biochemical failure after external beam radiotherapy changes conclusions about relative treatment efficacy for localized prostate cancer, *Urology* 68 (2006) 593–598, <https://doi.org/10.1016/j.urology.2006.03.075>.
- [5] C.R. Pound, A.W. Partin, M.A. Eisenberger, D.W. Chan, J.D. Pearson, P.C. Walsh, Natural history of progression after PSA elevation following radical prostatectomy, *JAMA* 281 (1999) 1591–1597.

- [6] Z.A. Siddiqui, D.J. Krauss, Adjuvant androgen deprivation therapy for prostate cancer treated with radiation therapy, *Transl. Androl. Urol.* 7 (2018) 378–389, <https://doi.org/10.21037/tau.2018.01.06>.
- [7] M.W. Kattan, J.A. Eastham, A.M. Stapleton, T.M. Wheeler, P.T. Scardino, A preoperative nomogram for disease recurrence following radical prostatectomy for prostate cancer, *J. Natl. Cancer Inst.* 90 (1998) 766–771, <https://doi.org/10.1093/jnci/90.10.766>.
- [8] M.W. Kattan, T.M. Wheeler, P.T. Scardino, Postoperative nomogram for disease recurrence after radical prostatectomy for prostate cancer, *J. Clin. Oncol.* 17 (1999) 1499–1507, <https://doi.org/10.1200/JCO.1999.17.5.1499>.
- [9] A.J. Stephenson, P.T. Scardino, J.A. Eastham, F.J. Bianco, Z.A. Dotan, C.J. DiBlasio, A. Reuther, E.A. Klein, M.W. Kattan, Postoperative nomogram predicting the 10-year probability of prostate cancer recurrence after radical prostatectomy, *J. Clin. Oncol.* 23 (2005) 7005–7012, <https://doi.org/10.1200/JCO.2005.01.867>.
- [10] Prostate Cancer Nomograms: Dynamic Prostate Cancer Nomogram: Coefficients | Memorial Sloan Kettering Cancer Center, (n.d.). https://www.mskcc.org/nomograms/prostate/pre_op/coefficients (accessed July 8, 2020).
- [11] T.A. Ozkan, A.T. Eruyar, O.O. Cebeci, O. Memik, L. Ozcan, I. Kuskonmaz, Interobserver variability in Gleason histological grading of prostate cancer, *Scand. J. Urol.* 50 (2016) 420–424, <https://doi.org/10.1080/21681805.2016.1206619>.
- [12] L. Pantanowitz, Digital images and the future of digital pathology, *J. Pathol. Inf.* 1 (2010), <https://doi.org/10.4103/2153-3539.68332>.
- [13] A. Tabesh, M. Teverovskiy, H.-Y. Pang, V.P. Kumar, D. Verbel, A. Kotsianti, O. Saidi, Multifeature prostate cancer diagnosis and Gleason grading of histological images, *IEEE Trans. Med. Imag.* 26 (2007) 1366–1378, <https://doi.org/10.1109/TMI.2007.898536>.
- [14] P. Leo, R. Elliott, N.N.C. Shih, S. Gupta, M. Feldman, A. Madabhushi, Stable and discriminating features are predictive of cancer presence and Gleason grade in radical prostatectomy specimens: a multi-site study, *Sci. Rep.* 8 (2018) 14918, <https://doi.org/10.1038/s41598-018-33026-5>.
- [15] P. Leo, A. Janowczyk, R. Elliott, N. Janaki, K. Bera, R. Shiradkar, X. Farré, P. Fu, A. El-Fahmawi, M. Shahait, J. Kim, D. Lee, K. Yamoah, T.R. Rebbeck, F. Khani, B.D. Robinson, L. Eklund, I. Jambor, H. Merisaari, O. Ettala, P. Taimen, H.J. Aronen, P.J. Boström, A. Tewari, C. Magi-Galluzzi, E. Klein, A. Purysko, N. Nc Shih, M. Feldman, S. Gupta, P. Lal, A. Madabhushi, Computer extracted gland features from H&E predicts prostate cancer recurrence comparably to a genomic companion diagnostic test: a large multi-site study, *Npj Prec. Oncol.* 5 (2021) 1–11, <https://doi.org/10.1038/s41698-021-00174-3>.
- [16] G. Lee, R. Sparks, S. Ali, N.N.C. Shih, M.D. Feldman, E. Spangler, T. Rebbeck, J.E. Tomaszewski, A. Madabhushi, Co-occurring gland angularity in localized subgraphs: predicting biochemical recurrence in intermediate-risk prostate cancer patients, *PLoS One* 9 (2014) e97954, <https://doi.org/10.1371/journal.pone.0097954>.
- [17] L. Boesen, N. Nørgaard, V. Løgager, I. Balslev, R. Bisbjerg, K.-C. Thstrup, M.D. Winther, H. Jakobsen, H.S. Thomsen, Assessment of the diagnostic accuracy of biparametric magnetic resonance imaging for prostate cancer in biopsy-Naive men: the biparametric MRI for detection of prostate cancer (BIDOC) study, *JAMA Netw. Open* 1 (2018) e180219, <https://doi.org/10.1001/jamanetworkopen.2018.0219>.
- [18] S. Woo, C.H. Suh, S.Y. Kim, J.Y. Cho, S.H. Kim, M.H. Moon, Head-to-Head comparison between biparametric and multiparametric MRI for the diagnosis of prostate cancer: a systematic review and meta-analysis, *Am. J. Roentgenol.* 211 (2018) W226–W241, <https://doi.org/10.2214/AJR.18.19880>.
- [19] S.K. Baruah, N. Das, S.J. Baruah, T.P. Rajeev, P.K. Bagchi, D. Sharma, M. Phukan, Combining prostate-specific antigen parameters with prostate imaging reporting and data System score version 2.0 to improve its diagnostic accuracy, *World J. Oncol.* 10 (2019) 218–225, <https://doi.org/10.14740/wjon1230>.
- [20] G.A. Sonn, R.E. Fan, P. Ghanouni, N.N. Wang, J.D. Brooks, A.M. Loening, B.L. Daniel, K.J. To'o, A.E. Thong, J.T. Leppert, Prostate magnetic resonance imaging interpretation varies substantially across radiologists, *Eur. Urol. Focus* 5 (2019) 592–599, <https://doi.org/10.1016/j.euf.2017.11.010>.
- [21] A. Cameron, F. Khalvati, M.A. Haider, A. Wong, MAPS: a quantitative radiomics approach for prostate cancer detection, *IEEE Trans. Biomed. Eng.* 63 (2016) 1145–1156, <https://doi.org/10.1109/TBME.2015.2485779>.
- [22] A. Alghary, R. Shiradkar, S. Pahwa, A. Purysko, S. Verma, D. Moses, R. Shnier, A.-M. Haynes, W. Delprado, J. Thompson, S. Tirumani, A. Mahran, A. R. Rastinehad, L. Ponsky, P.D. Stricker, A. Madabhushi, Combination of peri-tumoral and intra-tumoral radiomic features on Bi-parametric MRI accurately stratifies prostate cancer risk: a multi-site study, *Cancers* 12 (2020), <https://doi.org/10.3390/cancers12082200>.
- [23] B. Varghese, F. Chen, D. Hwang, S.L. Palmer, A.L. De Castro Abreu, O. Ukimura, M. Aron, M. Aron, I. Gill, V. Duddalwar, G. Pandey, Objective risk stratification of prostate cancer using machine learning and radiomics applied to multiparametric magnetic resonance images, *Sci. Rep.* 9 (2019) 1570, <https://doi.org/10.1038/s41598-018-38381-x>.
- [24] R. Shiradkar, S. Ghose, I. Jambor, P. Taimen, O. Ettala, A.S. Purysko, A. Madabhushi, Radiomic features from pretreatment biparametric MRI predict prostate cancer biochemical recurrence: preliminary findings, *J. Magn. Reson. Imag.* (2018), <https://doi.org/10.1002/jmri.26178>.
- [25] V. Bourbonne, M. Vallières, F. Lucia, L. Doucet, D. Visvikis, V. Tissot, O. Pradier, M. Hatt, U. Schick, MRI-derived radiomics to guide post-operative management for high-risk prostate cancer, *Front. Oncol.* 9 (2019) 807, <https://doi.org/10.3389/fonc.2019.00807>.
- [26] D. Sugano, A. Sidana, A.L. Jain, B. Calio, S. Gaur, M. Maruf, M. Merino, P. Choyke, B. Turkbey, B.J. Wood, P.A. Pinto, Index tumor volume on MRI as a predictor of clinical and pathologic outcomes following radical prostatectomy, *Int. Urol. Nephrol.* 51 (2019) 1349–1355, <https://doi.org/10.1007/s11255-019-02168-4>.
- [27] C. Magi-Galluzzi, A.J. Evans, B. Delahunt, J.I. Epstein, D.F. Griffiths, T.H. van der Kwast, R. Montironi, T.M. Wheeler, J.R. Grigley, L.L. Egevad, P.A. Humphrey, ISUP Prostate Cancer Group, International Society of Urological Pathology (ISUP), Consensus Conference on Handling and Staging of Radical Prostatectomy Specimens. Working group 3: extraprostatic extension, lymphovascular invasion and locally advanced disease, *Mod. Pathol.* 24 (2011) 26–38, <https://doi.org/10.1038/modpathol.2010.158>.
- [28] A.G. Wibmer, I. Nikolovski, J. Chaim, Y. Lakhman, R.A. Lefkowitz, E. Sala, S.V. Carlsson, S.W. Fine, M.W. Kattan, H. Hricak, H.A. Vargas, Local extent of prostate cancer at MRI versus prostatectomy histopathology: associations with long-term oncologic outcomes, *Radiology* 302 (2022) 595–602, <https://doi.org/10.1148/radiol.210875>.
- [29] M. Theiss, M.P. Wirth, A. Manseck, H.G. Frohmüller, Prognostic significance of capsular invasion and capsular penetration in patients with clinically localized prostate cancer undergoing radical prostatectomy, *Prostate* 27 (1995) 13–17, <https://doi.org/10.1002/pros.2990270104>.
- [30] Ş.L. Moroiaru, N. Bhattacharya, A. Seetharaman, W. Shao, C.A. Kunder, A. Sharma, P. Ghanouni, R.E. Fan, G.A. Sonn, M. Rusu, Computational detection of extraprostatic extension of prostate cancer on multiparametric MRI using deep learning, *Cancers* 14 (2022) 2821, <https://doi.org/10.3390/cancers14122821>.
- [31] R. Kikinis, S. Pieper, K. Vosburgh, 3D Slicer: a platform for subject-specific image analysis, visualization, and clinical support, *Intraoper. Imag. Image-Guided Ther.* (2014) 277–289.
- [32] A. Fedorov, M. Schmier, D. Clunie, C. Herz, S. Pieper, R. Kikinis, C. Tempany, F. Fennessy, An annotated test-retest collection of prostate multiparametric MRI, *Sci. Data* 5 (2018) 180281, <https://doi.org/10.1038/sdata.2018.281>.
- [33] A. Madabhushi, M. Feldman, in: *Fused Radiology-Pathology Prostate Dataset*, 2016, <https://doi.org/10.7937/K9/TCIA.2016.TLPMRIAM>.
- [34] A. Singanamalli, M. Rusu, R.E. Sparks, N.N.C. Shih, A. Ziober, L.-P. Wang, J. Tomaszewski, M. Rosen, M. Feldman, A. Madabhushi, Identifying in vivo DCE MRI markers associated with microvessel architecture and gleason grades of prostate cancer: MRI Markers of Microvessel Architecture in Prostate Cancer, *J. Magn. Reson. Imag.* 43 (2016) 149–158, <https://doi.org/10.1002/jmri.24975>.
- [35] R.J. Toth, N. Shih, J.E. Tomaszewski, M.D. Feldman, O. Kutter, D.N. Yu, J.C. Paulus, G. Paladini, A. Madabhushi, Histostitcher™: an informatics software platform for reconstructing whole-mount prostate histology using the extensible imaging platform framework, *J. Pathol. Inf.* 5 (2014) 8, <https://doi.org/10.4103/2153-3539.129441>.
- [36] G. Xiao, B.N. Bloch, J. Chappelow, E.M. Genega, N.M. Rofsky, R.E. Lenkinski, J. Tomaszewski, M.D. Feldman, M. Rosen, A. Madabhushi, Determining histology-MRI slice correspondences for defining MRI-based disease signatures of prostate cancer, *Comput. Med. Imag. Graph.* 35 (2011) 568–578, <https://doi.org/10.1016/j.compmedimag.2010.12.003>.
- [37] J. Chappelow, B.N. Bloch, N. Rofsky, E. Genega, R. Lenkinski, W. DeWolf, A. Madabhushi, Elastic registration of multimodal prostate MRI and histology via multiattribute combined mutual information: multiattribute combined mutual information, *Med. Phys.* 38 (2011) 2005–2018, <https://doi.org/10.1118/1.3560879>.
- [38] J.G. Sled, A.P. Zijdenbos, A.C. Evans, A nonparametric method for automatic correction of intensity nonuniformity in MRI data, *IEEE Trans. Med. Imag.* 17 (1998) 87–97, <https://doi.org/10.1109/42.668698>.
- [39] S. Klein, M. Staring, K. Murphy, M.A. Viergever, J.P.W. Pluim, elastix: a toolbox for intensity-based medical image registration, *IEEE Trans. Med. Imag.* 29 (2010) 196–205, <https://doi.org/10.1109/TMI.2009.2035616>.

- [40] D. Mattes, D.R. Haynor, H. Vesselle, T.K. Lewellen, W. Eubank, PET-CT image registration in the chest using free-form deformations, *IEEE Trans. Med. Imag.* 22 (2003) 120–128, <https://doi.org/10.1109/TMI.2003.809072>.
- [41] J.J.M. van Griethuysen, A. Fedorov, C. Parmar, A. Hosny, N. Aucoin, V. Narayan, R.G.H. Beets-Tan, J.-C. Fillion-Robin, S. Pieper, H.J.W.L. Aerts, Computational radiomics system to decode the radiographic phenotype, *Cancer Res.* 77 (2017) e104–e107, <https://doi.org/10.1158/0008-5472.CAN-17-0339>.
- [42] P. Prasanna, P. Tiwari, A. Madabhushi, Co-Occurrence of local anisotropic gradient orientations (CoLAGE): distinguishing tumor confounders and molecular subtypes on MRI, in: P. Golland, N. Hata, C. Barillot, J. Hornegger, R. Howe (Eds.), *Medical Image Computing and Computer-Assisted Intervention – MICCAI 2014*, Springer International Publishing, Cham, 2014, pp. 73–80. http://link.springer.com/10.1007/978-3-319-10443-0_10 (accessed October 19, 2016).
- [43] K.I. Laws, *Textured Image Segmentation*, University of Southern California, 1980.
- [44] I. Fogel, D. Sagi, Gabor filters as texture discriminator, *Biol. Cybern.* 61 (1989) 103–113, <https://doi.org/10.1007/BF00204594>.
- [45] A. Basavanthally, S. Ganesan, M. Feldman, N. Shih, C. Mies, J. Tomaszewski, A. Madabhushi, Multi-field-of-view framework for distinguishing tumor grade in ER + breast cancer from entire histopathology slides, *IEEE Trans. Biomed. Eng.* 60 (2013) 2089–2099, <https://doi.org/10.1109/TBME.2013.2245129>.
- [46] S. Ali, R. Veltri, J.A. Epstein, C. Christudass, A. Madabhushi, in: M.N. Gurcan, A. Madabhushi (Eds.), *Cell Cluster Graph for Prediction of Biochemical Recurrence in Prostate Cancer Patients from Tissue Microarrays*, 2013, p. 86760H, <https://doi.org/10.1117/12.2008695>.
- [47] R.M. Haralick, K. Shanmugam, I. Dinstein, Textural features for image classification, *IEEE Trans. Syst., Man, Cybern. SMC-3* (1973) 610–621, <https://doi.org/10.1109/TSMC.1973.4309314>.
- [48] S. Pölsterl, Scikit-survival: a library for time-to-event analysis built on top of scikit-learn, *J. Mach. Learn. Res.* 21 (2020) 1–6.
- [49] The UCSF Cancer of the Prostate Risk Assessment (CAPRA) Score: a straightforward and reliable preoperative predictor of disease recurrence after radical prostatectomy – PMC, (n.d.). <https://www.ncbi.nlm.nih.gov/pmc/articles/PMC2948569/> (accessed October 27, 2022).
- [50] Regression Shrinkage and Selection via the Lasso on JSTOR, (n.d.). <https://www.jstor.org/stable/2346178?seq=1> (accessed March 21, 2022).
- [51] E.W. Steyerberg, M.J.C. Eijkemans, F.E. Harrell Jr., J.D.F. Habbema, Prognostic modelling with logistic regression analysis: a comparison of selection and estimation methods in small data sets, *Stat. Med.* 19 (2000) 1059–1079, [https://doi.org/10.1002/\(SICI\)1097-0258\(20000430\)19:8<1059::AID-SIM412>3.0.CO;2-0](https://doi.org/10.1002/(SICI)1097-0258(20000430)19:8<1059::AID-SIM412>3.0.CO;2-0).
- [52] F.E. Harrell Jr., K.L. Lee, R.M. Califf, D.B. Pryor, R.A. Rosati, Regression modelling strategies for improved prognostic prediction, *Stat. Med.* 3 (1984) 143–152, <https://doi.org/10.1002/sim.4780030207>.
- [53] Using cross-validation to evaluate predictive accuracy of survival risk classifiers based on high-dimensional data – PMC, (n.d.). <https://www.ncbi.nlm.nih.gov/pmc/articles/PMC3105299/> (accessed October 27, 2022).
- [54] R. Ding, P. Prasanna, G. Corredor, C. Barrera, P. Zens, C. Lu, P. Velu, P. Leo, N. Beig, H. Li, P. Toro, S. Berezowska, V. Baxi, D. Balli, M. Belete, D.L. Rimm, V. Velcheti, K. Schalper, A. Madabhushi, Image analysis reveals molecularly distinct patterns of TILs in NSCLC associated with treatment outcome, *Npj Precis. Oncol.* 6 (2022) 33, <https://doi.org/10.1038/s41698-022-00277-5>.
- [55] N.D. James, M.R. Sydes, N.W. Clarke, M.D. Mason, D.P. Dearnaley, M.R. Spears, A.W.S. Ritchie, C.C. Parker, J.M. Russell, G. Attard, J. de Bono, W. Cross, R. J. Jones, G. Thalmann, C. Amos, D. Matheson, R. Millman, M. Alzouebi, S. Beesley, A.J. Birtle, S. Brock, R. Cathomas, P. Chakraborti, S. Chowdhury, A. Cook, T. Elliott, J. Gale, S. Gibbs, J.D. Graham, J. Hetherington, R. Hughes, R. Laing, F. McKinna, D.B. McLaren, J.M. O'Sullivan, O. Parikh, C. Peedell, A. Protheroe, A. J. Robinson, N. Srihari, R. Srinivasan, J. Staffurth, S. Sundar, S. Tolan, D. Tsang, J. Wagstaff, M.K.B. Parmar, STAMPEDE investigators, Addition of docetaxel, zoledronic acid, or both to first-line long-term hormone therapy in prostate cancer (STAMPEDE): survival results from an adaptive, multiarm, multistage, platform randomised controlled trial, *Lancet* 387 (2016) 1163–1177, [https://doi.org/10.1016/S0140-6736\(15\)01037-5](https://doi.org/10.1016/S0140-6736(15)01037-5).
- [56] D. Tilki, M.-H. Chen, J. Wu, H. Huland, M. Graefen, T. Wiegand, D. Böhmer, O. Mohamad, J.E. Cowan, F.Y. Feng, P.R. Carroll, B.J. Trock, A.W. Partin, A. V. D'Amico, Adjuvant versus early salvage radiation therapy for men at high risk for recurrence following radical prostatectomy for prostate cancer and the risk of death, *J. Clin. Orthod.* 39 (2021) 2284–2293, <https://doi.org/10.1200/JCO.20.03714>.
- [57] F.C. Hamdy, J.L. Donovan, J.A. Lane, M. Mason, C. Metcalfe, P. Holding, M. Davis, T.J. Peters, E.L. Turner, R.M. Martin, J. Oxley, M. Robinson, J. Staffurth, E. Walsh, P. Bollina, J. Catto, A. Doble, A. Doherty, D. Gillatt, R. Kockelbergh, H. Kynaston, A. Paul, P. Powell, S. Prescott, D.J. Rosario, E. Rowe, D.E. Neal, 10-year outcomes after monitoring, surgery, or radiotherapy for localized prostate cancer, *N. Engl. J. Med.* 375 (2016) 1415–1424, <https://doi.org/10.1056/NEJMoa1606220>.
- [58] J. Mikel Hubanks, S.A. Boorjian, I. Frank, M.T. Gettman, R. Houston Thompson, L.J. Rangel, E.J. Bergstralh, R. Jeffrey Karnes, The presence of extracapsular extension is associated with an increased risk of death from prostate cancer after radical prostatectomy for patients with seminal vesicle invasion and negative lymph nodes, *Urol. Oncol.* 32 (2014) 26.e1–26.e7, <https://doi.org/10.1016/j.urolonc.2012.09.002>.
- [59] D. Dalela, B. Löppenberg, A. Sood, J. Sammon, F. Abdollah, Contemporary role of the Decipher® test in prostate cancer management: current practice and future perspectives, *Rev. Urol.* 18 (2016) 1–9.
- [60] M. Covas Moschovas, C. Chew, S. Bhat, M. Sandri, T. Rogers, P. Dell'Oglio, S. Roof, S. Reddy, M.C. Sighinolfi, B. Rocco, V. Patel, Association between oncotype DX genomic prostate score and adverse tumor pathology after radical prostatectomy, S2405-4569(21)00094-8, *Eur Urol Focus* (2021), <https://doi.org/10.1016/j.euf.2021.03.015>.
- [61] A.E. Ross, M.H. Johnson, K. Yousefi, E. Davicioni, G.J. Netto, L. Marchionni, H.L. Fedor, S. Glavaris, V. Choeung, C. Buerki, N. Erho, L.L. Lam, E.B. Humphreys, S. Faraj, S.M. Bezerra, M. Han, A.W. Partin, B.J. Trock, E.M. Schaeffer, Tissue-based genomics augments post-prostatectomy risk stratification in a natural history cohort of intermediate- and high-risk men, *Eur. Urol.* 69 (2016) 157–165, <https://doi.org/10.1016/j.eururo.2015.05.042>.
- [62] D.E. Spratt, K. Yousefi, S. Dehesi, A.E. Ross, R.B. Den, E.M. Schaeffer, B.J. Trock, J. Zhang, A.G. Glass, A.P. Dicker, F. Abdollah, S.G. Zhao, L.L.C. Lam, M. du Plessis, V. Choeung, Z. Haddad, C. Buerki, E. Davicioni, S. Weinmann, S.J. Freedland, E.A. Klein, R.J. Karnes, F.Y. Feng, Individual patient-level meta-analysis of the performance of the decipher genomic classifier in high-risk men after prostatectomy to predict development of metastatic disease, *J. Clin. Oncol.* 35 (2017) 1991–1998, <https://doi.org/10.1200/JCO.2016.70.2811>.
- [63] A. Hiremath, R. Shiradkar, P. Fu, A. Mahran, A.R. Rastinehad, A. Tewari, S.H. Tirumani, A. Purysko, L. Ponsky, A. Madabhushi, An integrated nomogram combining deep learning, Prostate Imaging–Reporting and Data System (PI-RADS) scoring, and clinical variables for identification of clinically significant prostate cancer on biparametric MRI: a retrospective multicentre study, *Lancet Digit. Health* 3 (2021) e445–e454, [https://doi.org/10.1016/S2589-7500\(21\)00082-0](https://doi.org/10.1016/S2589-7500(21)00082-0).
- [64] A. Hiremath, R. Shiradkar, H. Merisaari, P. Prasanna, O. Ettala, P. Taimen, H.J. Aronen, P.J. Boström, I. Jambor, A. Madabhushi, Test-retest repeatability of a deep learning architecture in detecting and segmenting clinically significant prostate cancer on apparent diffusion coefficient (ADC) maps, *Eur. Radiol.* (2020), <https://doi.org/10.1007/s00330-020-07065-4>.
- [65] L. Li, R. Shiradkar, P. Leo, A. Alghohary, P. Fu, S.H. Tirumani, A. Mahran, C. Buzzy, V.C. Obmann, B. Mansoori, A. El-Fahmawi, M. Shahait, A. Tewari, C. Magi-Galluzzi, D. Lee, P. Lal, L. Ponsky, E. Klein, A.S. Purysko, A. Madabhushi, A novel imaging based Nomogram for predicting post-surgical biochemical recurrence and adverse pathology of prostate cancer from pre-operative bi-parametric MRI, *EBioMedicine* 63 (2021) 103163, <https://doi.org/10.1016/j.ebiom.2020.103163>.
- [66] R. Shiradkar, S. Ghose, A. Mahran, L. Li, I. Hubbard, P. Fu, S.H. Tirumani, L. Ponsky, A. Purysko, A. Madabhushi, Prostate surface distension and tumor texture descriptors from pre-treatment MRI are associated with biochemical recurrence following radical prostatectomy: preliminary findings, *Front. Oncol.* 12 (2022) 841801, <https://doi.org/10.3389/fonc.2022.841801>.
- [67] G. Lee, A. Singanamalli, H. Wang, M.D. Feldman, S.R. Master, N.N.C. Shih, E. Spangler, T. Rebbeck, J.E. Tomaszewski, A. Madabhushi, Supervised multi-view canonical correlation analysis (smVCCA): integrating histologic and proteomic features for predicting recurrent prostate cancer, *IEEE Trans. Med. Imag.* 34 (2015) 284–297, <https://doi.org/10.1109/TMI.2014.2355175>.
- [68] L. Feng, Z. Liu, C. Li, Z. Li, X. Lou, L. Shao, Y. Wang, Y. Huang, H. Chen, X. Pang, S. Liu, F. He, J. Zheng, X. Meng, P. Xie, G. Yang, Y. Ding, M. Wei, J. Yun, M.-C. Hung, W. Zhou, D.R. Wahl, P. Lan, J. Tian, X. Wan, Development and validation of a radiopathomics model to predict pathological complete response to neoadjuvant chemoradiotherapy in locally advanced rectal cancer: a multicentre observational study, *Lancet Digit. Health* 4 (2022) e8–e17, [https://doi.org/10.1016/S2589-7500\(21\)00215-6](https://doi.org/10.1016/S2589-7500(21)00215-6).

- [69] P. Vaidya, X. Wang, K. Bera, A. Khunger, H. Choi, P. Patil, V. Velcheti, A. Madabhushi, RaPtomics: integrating radiomic and pathomic features for predicting recurrence in early stage lung cancer, in: *Medical Imaging 2018: Digital Pathology*, International Society for Optics and Photonics, 2018, p. 105810M, <https://doi.org/10.1117/12.2296646>.
- [70] S. Rathore, A. Chaddad, M.A. Iftikhar, M. Bilello, A. Abdulkadir, Combining MRI and histologic imaging features for predicting overall survival in patients with glioma, *Radiol.: Imaging Cancer* 3 (2021) e200108, <https://doi.org/10.1148/rycan.2021200108>.
- [71] W. Shao, Z. Han, J. Cheng, L. Cheng, T. Wang, L. Sun, Z. Lu, J. Zhang, D. Zhang, K. Huang, Integrative analysis of pathological images and multi-dimensional genomic data for early-stage cancer prognosis, *IEEE Trans. Med. Imag.* 39 (2020) 99–110, <https://doi.org/10.1109/TMI.2019.2920608>.
- [72] N. Braman, J.W.H. Gordon, E.T. Goossens, C. Willis, M.C. Stumpe, J. Venkataraman, Deep orthogonal fusion: multimodal prognostic biomarker discovery integrating radiology, pathology, genomic, and clinical data, in: M. de Bruijne, P.C. Cattin, S. Cotin, N. Padoy, S. Speidel, Y. Zheng, C. Essert (Eds.), *Medical Image Computing and Computer Assisted Intervention – MICCAI 2021*, Springer International Publishing, Cham, 2021, pp. 667–677, https://doi.org/10.1007/978-3-030-87240-3_64.
- [73] S.D. McGarry, J.D. Bukowy, K.A. Iczkowski, A.K. Lowman, M. Brehler, S. Bobholz, A. Nencka, A. Barrington, K. Jacobsohn, J. Unteriner, P. Duvnjak, M. Griffin, M. Hohenwalter, T. Keuter, W. Huang, T. Antic, G. Paner, W. Palangmonthip, A. Banerjee, P.S. LaViolette, Radio-pathomic mapping model generated using annotations from five pathologists reliably distinguishes high-grade prostate cancer, *J. Med. Imaging* 7 (2020) 054501, <https://doi.org/10.1117/1.JMI.7.5.054501>.
- [74] R. Shiradkar, A. Panda, P. Leo, A. Janowczyk, X. Farre, N. Janaki, L. Li, S. Pahwa, A. Mahran, C. Buzzy, P. Fu, R. Elliott, G. MacLennan, L. Ponsky, V. Gulani, A. Madabhushi, T1 and T2 MR fingerprinting measurements of prostate cancer and prostatitis correlate with deep learning-derived estimates of epithelium, lumen, and stromal composition on corresponding whole mount histopathology, *Eur. Radiol.* (2020), <https://doi.org/10.1007/s00330-020-07214-9>.
- [75] P. Mobadersany, S. Yousefi, M. Amgad, D.A. Gutman, J.S. Barnholtz-Sloan, J.E. Velázquez Vega, D.J. Brat, L.A.D. Cooper, Predicting cancer outcomes from histology and genomics using convolutional networks, *Proc. Natl. Acad. Sci. U. S. A.* 115 (2018) E2970–E2979, <https://doi.org/10.1073/pnas.1717139115>.
- [76] R.J. Chen, M.Y. Lu, J. Wang, D.F.K. Williamson, S.J. Rodig, N.I. Lindeman, F. Mahmood, Pathomic fusion: an integrated framework for fusing histopathology and genomic features for cancer diagnosis and prognosis, *IEEE Trans. Med. Imag.* 41 (2022) 757–770, <https://doi.org/10.1109/TMI.2020.3021387>.
- [77] J.J. Kang, R. Reiter, M. Steinberg, C.R. King, Ultra-sensitive PSA following prostatectomy reliably identifies patients requiring post-op radiotherapy, *J. Urol.* 193 (2015) 1532–1538, <https://doi.org/10.1016/j.juro.2014.11.017>.